Shape-induced chiral ordering in two-dimensional packing of snowmanlike dimeric particles

Youngkyu Han,[1,*] Juncheol Lee,[2] Siyoung Q. Choi,[3] Myung Chul Choi,[2] and Mahn Won Kim[1,4,†]
[1]*Department of Physics, KAIST, Daejeon 305-701, Korea*
[2]*Department of Bio and Brain Engineering, KAIST, Daejeon 305-701, Korea*
[3]*Information Electrical Research Institute, KAIST, Daejeon 305-701, Korea*
[4]*Institute for Soft and Bio Matter Science, Changwon National University, Changwon 641-773, Korea*
(Received 28 May 2013; published 11 October 2013)

Understanding the distinctive phase behaviors in random packing due to particle shapes is an important issue in condensed matter physics. In this paper, we investigate the random packing structure of two-dimensional (2D) snowmen via wax-snowman packing experiments and Brownian dynamics simulations. Both experiments and simulations reveal that neighboring snowmen have a strong short-range orientational correlation and consequently locally form particular conformations. A chiral conformation is dominant for high area fractions near the jamming condition ($\varphi > 0.8$), and the proportion of the chiral conformation increases with γ. We also found that the attractive interaction does not have a significant impact on the results. The geometry of chirally ordered snowmen causes a mismatch with 2D crystalline symmetries and thus inhibits the development of long-range spatial order, despite the strong orientational correlation between neighbors.

DOI: 10.1103/PhysRevE.88.042202 PACS number(s): 45.70.−n, 64.60.Cn, 63.50.Lm, 83.10.Mj

I. INTRODUCTION

Dense random packing of hard particles is a fundamental problem in condensed matter physics. In recent decades a great deal of study has been dedicated using the hard particle systems [1–6] to understand the underlying mechanisms of physical phenomena such as melting [7], jamming [8–10], and glass transitions [11–13] in a variety of systems. In random packing of hard particles, the geometry of particles including shape and size plays a crucial role in determining phases of systems as well as microscopic structures [14–23]. For example, a binary system composed of two kinds of particles of different sizes shows remarkably distinctive phases and structures from a system of identical particles; binary disks exhibit more complicated phases including various superlattices [24,25], and remain in a glassy phase even at higher densities, compared to monodisperse disks [26–29].

A two-dimensional (2D) system of snowman-shaped dimeric particles (called "snowmen") is a good model to demonstrate the importance of both size and shape anisotropy of hard particles. This snowman system is composed of anisotropic particles in 2D, each of which consists of a pair of binary disks connected by a bond. Various 2D snowman shapes can be generated by varying the head-to-body radius ratio γ ($=R_h/R_b$) from 0 to 1 [Fig. 1 (a)], where R_b is the radius of the larger disk (body) and R_h is that of the smaller disk (head). These 2D snowman shapes are suitable to tile the 2D space so that we can construct several types of periodic packing structures. Such periodic packings of snowmen resemble those of binary disks [24,25]. Figures 1(b)–1(i) show the compact periodic packing configurations of 2D snowmen, which correspond to the particular γ's where both the mean coordination number and the occupied area fraction φ are maximized. On the other hand, a bond—the characteristic that distinguishes snowman shapes from binary disks—remarkably changes the local structure and phase behavior if snowmen are randomly assembled. While binary disks exhibit a continuous jammed states spectrum from the maximally random jammed (MRJ) state to the phase-separated crystal state without an ideal glass transition [27,28], the existence of a bond in snowmen prohibits local segregation of constituent disks of snowmen and reduces the jammed phase spectrum [23].

Previously, Han and Kim [23] discussed the effect of 2D snowman shapes on the packing structure at different length scales near the MRJ state. In their paper, the spatial ordering between snowmen was suppressed as the shape became asymmetric by changing γ from 0 or 1. Thus, asymmetric snowmen fail to attain ordered structures even at high area fractions near the MRJ fraction ($\varphi \sim 0.84$), contrary to the symmetric snowmen ($\gamma = 0$ and 1) where a disorder-order transition exists. Snowmen with large γ (=0.5 and 0.7) were strongly correlated with the surrounding particles in their orientation. A question arises from these results: Why does such a strong orientational correlation leave snowman particles to be disordered?

In this paper, we investigate the structure of random packing of 2D asymmetric snowman particles and present the key findings. We characterize the amorphous structure of a 2D monolayer of wax snowman particles in terms of the relative position and orientation between the nearest neighbors. First, we show that two neighboring snowmen preferentially form particular conformations (named "patterns"), having certain angles: parallel (P), antiparallel (A_{I} and A_{II}), and chiral (C) patterns (Sec. III). Second, we find that the chiral conformation is dominant in random jammed packing of snowmen. Additionally, by performing Brownian dynamics (BD) simulations, we demonstrate that the preference for chiral ordering in snowman packing is not related to the type of short-range interaction between particles and increases with γ (Sec. IV). These findings are intriguing because only the chiral conformation does not fit 2D crystalline symmetries contrary to the other three patterns. We suggest

*ykhan@kaist.ac.kr
†Also at Gwangju Institute of Science and Technology, Gwangju 500-712, Korea; mwkim@kaist.ac.kr

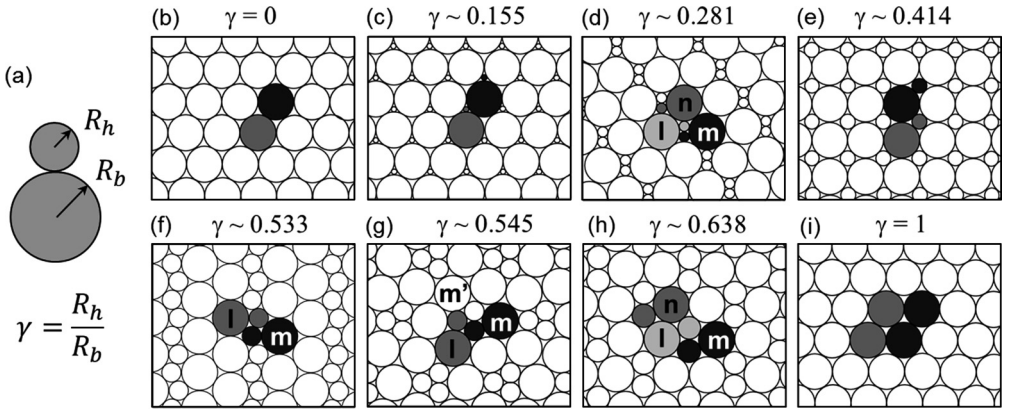

FIG. 1. (a) A 2D snowman shape is characterized by γ, which is the radius ratio between its head (smaller) and its body (larger disk). (b)–(i) Regularly tiled structures of 2D snowmen for particular γ values, where the mean coordination number and the area fraction per particle are maximized. These periodic configurations can be divided into identical tiling-units: individual snowmen for panels (b), (c), (e), and (i); l-m or l-n units for panels (d), (f), and (h); and l-m-m′ units for (g).

that the preference for local chiral ordering inhibits the development of long-range spatial order in random snowman packing despite the strong orientational correlation between neighbors.

II. EXPERIMENTAL SYSTEMS AND SIMULATION DETAILS

A. Experiment

Our experiments are performed using flat and thin snowman platelets, which are floating at the air-water interface. The fabrication and packing of 2D wax-snowman particles are described in Ref. [23]. Paraffin wax is melted in a flat dish and cut by a snowman-shaped cutter. Snowman particles with three different head-to-body radius ratios, γ (=0.3, 0.5, and 0.7), are produced, and they are mono-dispersed in size and shape; the snowman-body radius R_b is fixed at 10 mm (R_h varied only) and the thickness is about 3 mm. The particles are spread on water in a trough (430 × 400 mm^2 inner area) and float because they are hydrophobic and slightly lighter than water. The snowmen in our experiment have short-range attraction with other particles due to capillary interaction [23,30–32] and can be regarded as non-Brownian particles because of their large size. The area fraction φ is controlled either by changing the number of particles or by moving a barrier. A random configuration is generated by perturbation, such as stirring by tweezers and gentle shaking for less than a minute with an amplitude of a few centimeters. As a result, the particles are randomly dispersed without any preference in their positions and orientations, and the newly obtained configuration is independent of previous ones. As shown in Figs. 2(a) and 2(b), each configuration of snowmen is recorded by a webcam. To obtain positions and orientations of the snowmen, each snowman is labeled by a pair of distinguishable dots—one at the center of a body and the other at the point where a body and its head meet. Figures 2(a) and 2(b) show the results of our image processing, and an actual snowman particle labeled by the dots is presented in the inset of Fig. 2(a).

B. Brownian dynamics simulation

We perform BD simulations [33] to study packing of 2D snowmen with $\gamma = 0.3$, 0.5, and 0.7. Four-hundred snowmen are initially located at the square lattice sites within a region enclosed by four walls on each side and compressed by moving the walls during the packing process. The positions of walls

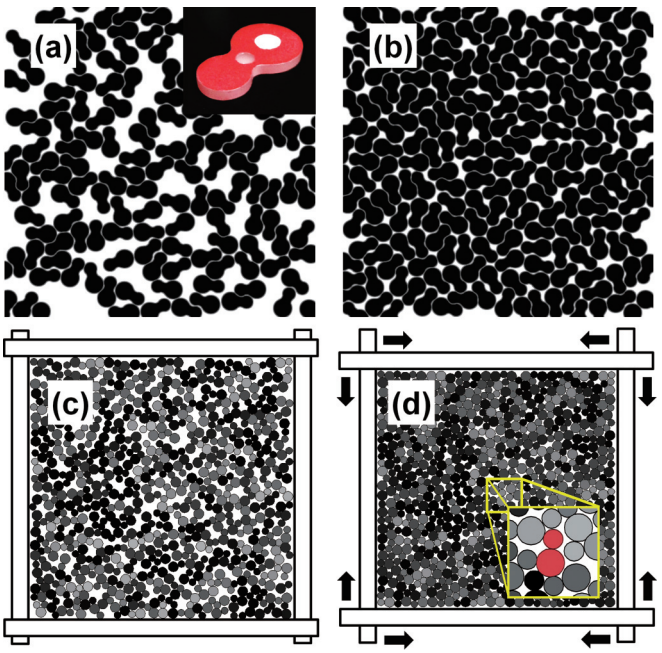

FIG. 2. (Color online) (a) and (b) Experimental results of random packing configurations at the area fraction $\varphi = 0.66$ (a) and 0.83 (b). These binary images are obtained by image processing the raw image data. A bird's eye view of an actual snowman particle labeled by dots is shown in the inset of panel (a). (c) and (d) BD simulation results at area fractions $\varphi = 0.66$ (c) and 0.83 (d). By moving walls (white rectangles) on each side, systems are compressed from the initial area fraction φ_{initial} to the final area fraction φ_{final}. Snowmen are distinguishable from neighbors by different gray scales. The inset shows a zoomed-in image of the region in the yellow box. $\gamma = 0.7$ in panels (a)–(d).

and snowmen are updated at each time step Δt. The new position of each snowman, $x_i(t+\Delta t)$, is computed using the over-damped Brownian dynamics with thermal fluctuation, $R(t)$, and the sum of all interaction forces exerted on the snowman, F_i,

$$x_i(t+\Delta t) = x_i(t) + \frac{F_i}{\zeta}\Delta t + \sqrt{2DR(t)}, \tag{1}$$

where ζ is the friction constant coefficient of snowmen, $D = k_B T/\zeta$ is the diffusion constant, and $R(t)$ is a δ-correlated stationary Gaussian process with zero mean and satisfies $\langle R(t)\rangle = 0$ and $\langle R(t)R(t')\rangle = \delta(t-t')$. The interaction force between two snowmen is the vector sum of forces between their constituent disks $F_{jk} = -\nabla U_{jk}$, and U_{jk} is a Lennard-Jones-type interaction,

$$U_{jk} = \epsilon\left(\frac{R_{jk}}{2R_b}\right)\left\{\left(\frac{R_{jk}}{r}\right)^{12} - 2\left(\frac{R_{jk}}{r}\right)^{6}\right\}\Theta(R_{jk}-r). \tag{2}$$

Here, ϵ is the interaction strength and $\Theta(R_{jk}-r)$ is the Heaviside step function, such that snowman particles interact only when they overlap each other. For two disks j and k from two distinct snowmen, r is the distance between their centers and R_{jk} is the contact distance, given as follows

$$R_{jk} = \begin{cases} 2\gamma R_b & \text{if } j \text{ and } k \text{ are heads,} \\ (1+\gamma)R_b & \text{if } j \text{ is a body and } k \text{ is a head} \\ & \text{or vice versa,} \\ 2R_b & \text{if } j \text{ and } k \text{ are bodies,} \end{cases} \tag{3}$$

where R_b is the radius of bodies. The interaction between walls and snowmen is the same as the Lennard-Jones-type potential, which is only dependent on the distance between them.

As the four walls start moving toward the center of the system at a constant speed, v, regardless of the motion of snowman particles, the system is compressed from the initial area fraction $\varphi_{\text{initial}} \sim 0.3$ to the final area fraction $\varphi_{\text{final}} = 0.9$. The compression rate, related to a dimensionless number, $Pe = va/D \sim 1$, is sufficient to make the particles evenly distributed over the system by Brownian relaxation without crowding near the walls, where a is the particle size and D is the diffusion constant. The simulation constants are chosen to avoid too much overlap of snowman particles as well as inhomogeneous packing: $k_B T = 0.025\ \epsilon$, $\zeta = \epsilon t_0/R_b^2$, and $t_0 = 2\times 10^{-4}$, where t_0 is the time required for a particle to diffuse as far as its radius. Particles do not overlap with their neighbors by more than a few percent of their radius on average under these conditions. Additionally, at lower density ($\varphi < 0.7$) the effective temperature is increased tenfold for a faster packing process.

We perform BD simulations under two different conditions: soft-core particles with and without short-range attraction. First, we use purely repulsive soft-core particles by cutting the potential where the repulsive force between neighboring particles is zero [Eq. (2)]. Second, we use soft-core particles with Lennard-Jones-type short-range attraction. We add an attractive interaction between the repulsive soft-core particles by modifying the original step function of Eq. (2).

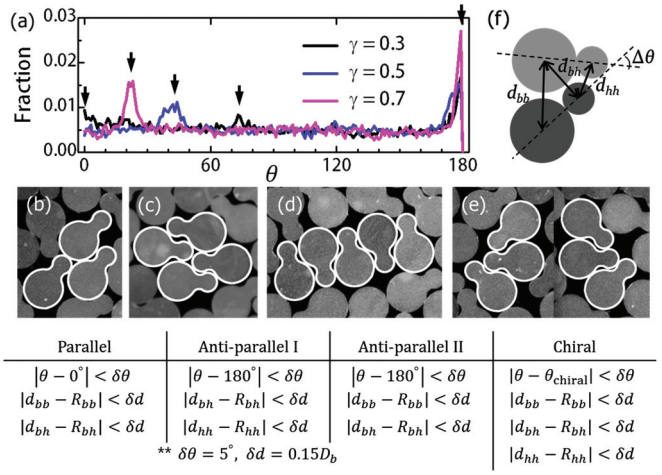

Parallel	Anti-parallel I	Anti-parallel II	Chiral
$\lvert\theta - 0^\circ\rvert < \delta\theta$	$\lvert\theta - 180^\circ\rvert < \delta\theta$	$\lvert\theta - 180^\circ\rvert < \delta\theta$	$\lvert\theta - \theta_{\text{chiral}}\rvert < \delta\theta$
$\lvert d_{bb} - R_{bb}\rvert < \delta d$	$\lvert d_{bh} - R_{bh}\rvert < \delta d$	$\lvert d_{bb} - R_{bb}\rvert < \delta d$	$\lvert d_{bb} - R_{bb}\rvert < \delta d$
$\lvert d_{bh} - R_{bh}\rvert < \delta d$	$\lvert d_{hh} - R_{hh}\rvert < \delta d$	$\lvert d_{bh} - R_{bh}\rvert < \delta d$	$\lvert d_{bh} - R_{bh}\rvert < \delta d$
	** $\delta\theta = 5^\circ$, $\delta d = 0.15 D_b$		$\lvert d_{hh} - R_{hh}\rvert < \delta d$

FIG. 3. (Color online) (a) The distribution of angle θ between two neighboring snowmen $\gamma = 0.3$ (black), 0.5 (blue or gray), and 0.7 (magenta or light gray) at the MRJ fraction ($\varphi_{\text{MRJ}} \sim 0.84$) from random packing experiments. (b)–(e) Snapshots of local configurations of the snowman particles ($\gamma = 0.5$). The highlighted snowmen are of particular angle differences: $\theta_{\text{peak}} = 0^\circ$ [panel (b)]; 180° [panels (c) and (d); and 23°, 45°, and 74° [panel (e)]. Four types of "patterns" are defined from these θ_{peak}: (b) parallel, (c) antiparallel I, (d) antiparallel II, and (e) chiral patterns. (f) The criterion for classification, whether two snowmen form one of the particular patterns or not, is based on θ and d_{bb}, d_{bh}, and d_{hh}, which are the distances between two bodies, one body and one head, and two heads, respectively.

III. OBSERVATION OF CHIRAL ORDERING IN 2D SNOWMAN PACKING EXPERIMENT

Han and Kim [23] previously reported that asymmetric snowmen remain disordered even at high φ, while disks and dimers ($\gamma = 0,1$) undergo a disorder-order transition. As γ increases from 0 or decreases from 1, a snowman shape becomes more asymmetric and interferes with the hexagonal crystalline packing that can be achieved using disks and dimers [24,25,34].

On the other hand, orientations of snowmen are correlated with their nearest neighbors, as seen by the distribution of angle θ between nearest-neighboring snowmen at the MRJ fraction ($\varphi \sim 0.84$) for three different size ratios γ's (=0.3, 0.5, and 0.7) in Fig. 3(a). There exist several peaks at $\theta_{\text{peak}} = 0^\circ$, 23°, 45°, 74°, and 180°. We find that two of these peaks, 0° and 180°, appear in the relative orientation between nearest neighbors in the 2D *periodic* snowman packing [Figs. 1(b)–1(i)]. Each packing configuration can be divided into identical tiling blocks comprised of neighboring pairs. A snowman pair with a zero angle difference can form a parallel conformation, as indicated by the two labeled snowmen shown in Figs. 1(c) and 1(e). A pair with a 180° angle difference can be matched to antiparallel conformations such as either l-m or l-n pairs in Figs. 1(d), 1(f), and 1(h). Figures 3(b)–3(d) show examples of such particular conformations with $\theta = 0^\circ$ and 180°. In addition, one more conformation corresponding to the other $\theta_{\text{peak}} = 23^\circ$, 45°, and 74° appears when neighboring snowmen with $\gamma = 0.3$, 0.5, or 0.7 are in tight contact as shown in

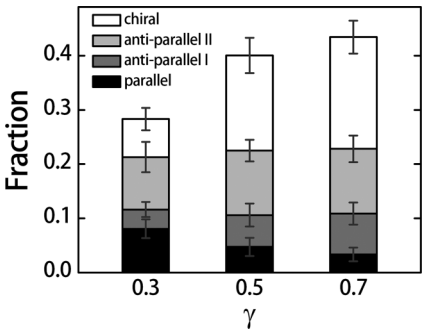

FIG. 4. The distribution of the particular patterns at the MRJ fraction for $\gamma = 0.3$, 0.5, and 0.7 in wax-snowman packing experiments. From bottom to top: parallel (black), antiparallel I (dark gray), antiparallel II (gray), and chiral (white) patterns. As γ increases, the total amount of all the patterns exceeds 0.4, and the chiral pattern is preferred most.

Fig. 3(e). This conformation is named *chiral* because it has two distinct possibilities due to mirror symmetry.

Considering the θ_{peak}, we defined four particular conformations (called patterns) of neighboring snowmen—parallel (P), antiparallel I (A_I) and II (A_{II}), and chiral (C) patterns, in Figs. 3(b)–3(e), respectively. We set criteria to categorize each neighboring pair into four types of patterns by using the relative positions and orientations between two snowmen, which include the angle difference θ, the distance between two bodies (d_{bb}) and two heads (d_{hh}), and the shorter distance between one's body and the other's head (d_{bh}) as shown in Fig. 3(f). Small deviations from the ideal pattern conformations are allowed as shown in the table of Fig. 3; $|\theta - \theta_{\text{peak}}| < \delta\theta$ and $|d_{kj} - R_{jk}| < \delta d$, where $D_b = 2R_b$, and j and k are constituent disks. We decide the marginal angle difference, $\delta\theta$, from the peak widths of θ_{peak} and the marginal distance, δd, from the criteria for particle-particle contact determination [23]: $\delta\theta = 5^\circ$ and $\delta d = 0.15D_b$ in data analysis for the experiments. Variations of the marginal values within $\delta d < 0.15D_b$ do not affect the overall tendency in pattern distributions, and $\delta\theta$ is fixed. There is no significant difference in the criteria between the four patterns.

In Fig. 4, we present the distribution of four particular patterns in random packing of snowmen with $\gamma = 0.3$, 0.5, and 0.7 at the MRJ fraction. The proportion of each pattern is defined as $N_{\text{pattern}}/N_{\text{total}}$, where N_{pattern} is the number of snowmen assembling the pattern and N_{total} is the total number of particles. A small fraction of the snowmen are double counted because they form more than one pattern with different neighbors simultaneously, 2.1%, 3.4%, and 3.5% for $\gamma = 0.3$, 0.5, and 0.7, respectively. Other snowmen of $1 - \sum N_{\text{pattern}}/N_{\text{total}}$ are in contact with their neighbors with random orientations, except for θ_{peak}. The distribution of each pattern exhibits γ dependence in detail; as γ increases, pattern P decreases, pattern A_{II} is nearly unchanged, and the others increase. Interestingly, the chiral pattern is the most dominant pattern in the structures of random snowman packing. This chiral pattern cannot fit in 2D crystalline symmetries, contrary to the other patterns. The mismatch between the locally favored structure and 2D symmetries inhibits the system from developing long-range spatial order except for the case of $\gamma = 1$, where the chiral pattern and the others become identical so that particles exhibit quasi-long-range bond order [23,34]. Therefore, this suggests that the preference for chiral ordering between snowmen can be a key factor in explaining why snowman particles remain disordered at high φ despite their strong orientational correlation with their neighbors.

IV. PREFERENCE FOR LOCAL CHIRAL ORDERING AND ITS STABILITY

Short-range attractive forces act on the snowman particles located at the air-water interface due to the capillary interaction [23]. Unfortunately, we cannot check how the attraction affects the local ordering between neighbors in our packing experiments, because it is difficult to completely remove the attractive interaction between the particles floating on water surfaces. We perform BD simulations under two different conditions instead—snowman particles with and without short-range attractive interaction, as described in Sec. II B. The attractive potential of the soft-core particles is stronger than the given thermal energy and also longer ranged than capillary attraction between wax snowman particles; $\epsilon = 40$ k_BT and the cutoff length ξ_{cutoff} ($\sim D_b$) is greater than the capillary length ξ_{capil} ($\sim 0.1D_b$) [23].

To see the effect of this attractive interaction on the packing structure, systems with two different interactions at $\varphi = 0.85$ are compared via the radial correlation function $g(r)$ and the bond-orientational correlation function $g_6(r)$ for the center-of-mass of snowmen, as shown in Fig. 5. The $g_6(r)$ is defined

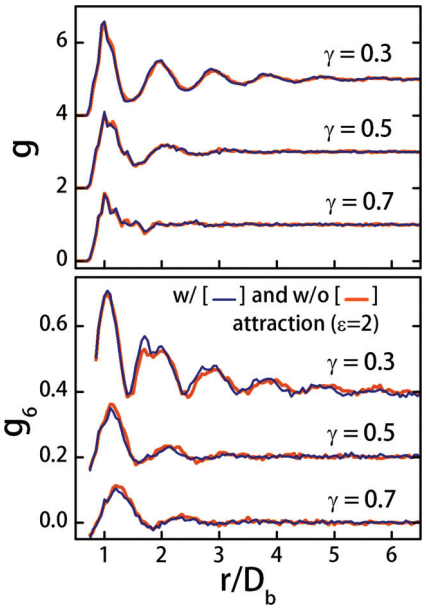

FIG. 5. (Color online) (a) Radial correlation function g and (b) sixfold bond-orientational correlation function g_6 near the MRJ fraction ($\varphi = 0.85$) from BD simulations. Simulations are performed under two different conditions by modifying the Lennard-Jones-type potential: soft-core interaction without attraction (orange or light gray) and with short-range and weak attraction (navy or dark gray). There is no significant difference between the two cases. The graphs are vertically shifted for clarity: $\gamma = 0.3$, 0.5, and 0.7 from top to bottom. The distance is normalized by $D_b = 2R_b$, and the strength of the Lennard-Jones potential $\epsilon = 2$.

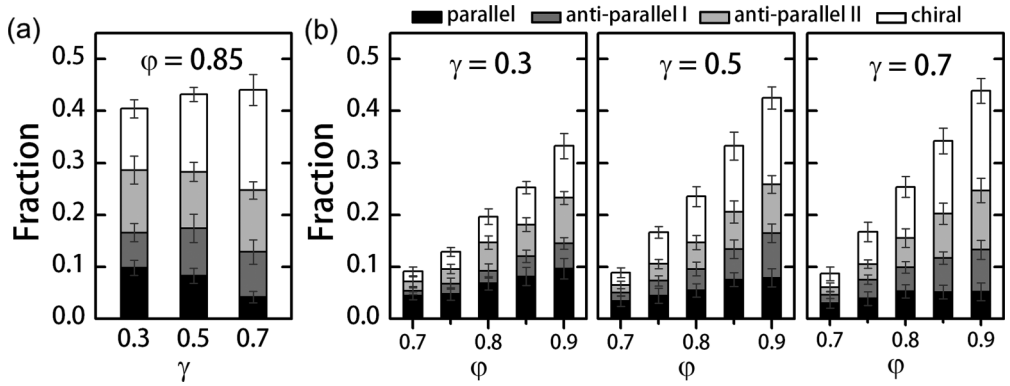

FIG. 6. The distribution of the patterns for $\gamma = 0.3$, 0.5, and 0.7 from BD simulations with two different conditions: snowman particles (a) with attraction and (b) without attraction. Parallel (black), antiparallel I (dark gray), antiparallel II (gray), and chiral (white) patterns from bottom to top. (a) The pattern distribution at $\varphi = 0.85$. Similar to the experimental results in Fig. 4, the chiral pattern is dominant compared with other pattern types at a high fraction ($\varphi = 0.85$). (b) The pattern distribution at $\varphi = 0.7$–0.9. As φ increases, the fractions for all the patterns dramatically increase. Regardless of the existence of short-range attraction, the chiral pattern is the most preferred conformation.

as [16,19]

$$g_6(r) = \mathrm{Re}\langle \psi_6^*(0)\psi_6(r)\rangle, \tag{4}$$

with a local bond order parameter,

$$\psi_6(r_j) = \frac{1}{N_j}\sum_{k=1}^{N_j} e^{i6\theta_{jk}(r_j)}, \tag{5}$$

where N_j is the number of neighbors of the particle j, $\theta_{jk}(r_j)$ is the angle between a vector connecting the center-of-mass of particles j and k and an arbitrary fixed axis. All the correlation functions for $\gamma = 0.3$, 0.5, and 0.7 have a few peaks, which exponentially decay within a distance of less than several-particle diameters, and the peaks decay faster and become weaker at high γ. This is consistent with the previous experimental results [23] in the positions and decaying range of the peaks, except that the peaks of g and g_6 are broadened and weakened because the soft-core interaction allows the particles to be slightly overlapped. Meanwhile, in the correlation functions, there are no significant differences between the two disordered structures of the cases with and without attraction.

The two systems, however, show differences in terms of the pattern distribution. The total fraction of patterns for the system with attractive interaction is slightly greater than that of the nonattractive case, as presented in Figs. 6(a) and 6(b); the total fraction is about 0.45 for the attractive system and 0.35 for the nonattractive system at $\varphi = 0.85$. Nevertheless, the relative fractions of the four patterns are quite similar, and the fraction of the chiral pattern is dominant for both the attractive and the nonattractive systems. These findings imply that snowmen may favor the local chiral ordering between neighbors in random packing regardless of attractive interactions.

In Fig. 6(b), we present the change of the pattern distribution during the packing process ($\varphi = 0.7$–0.9) in nonattractive soft-core snowman systems. At $\varphi = 0.7$, only 10% of snowmen in the system form patterns because the particles are not in close contact with their neighbors at low densities. As φ increases, the particles become closer to each other and orientational degrees of freedom are reduced by their neighbors. These changes result in a drastic increment of the number of patterns. For the system with short-range attraction, attractive forces cause the snowmen to come into contact with surrounding particles at φ lower than that in the nonattractive case. This early formation of snowman aggregates induces a difference in the total fraction of patterns between attractive and nonattractive cases, as mentioned above. The chiral pattern becomes the largest fraction among the particular patterns as φ approaches the jamming condition, especially for the large γ's (=0.5 and 0.7).

In Fig. 7, we present how the proportion of the chiral pattern changes with increasing γ from 0.3 to 0.7 at $\varphi = 0.85$. At $\gamma = 0.3$, the chiral pattern is equally favored with the ordered patterns. However, the fraction of the chiral pattern increases with γ and becomes dominant; the increment of the fraction is more rapid at $\gamma = 0.3$–0.5. This γ dependency is in contrast to the other patterns; the parallel pattern decreases and the antiparallel patterns show an insignificant change. This preference for chiral ordering depending on γ is consistent with the experimental results in Sec. III. Moreover, this also can be also related to our suggestion at the end of Sec. III; as more snowman form the chiral pattern, the system becomes more structureless, although the orientational correlation becomes

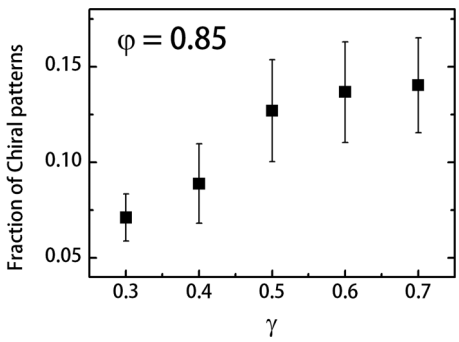

FIG. 7. The proportion of the chiral pattern depending on γ at $\varphi = 0.85$. As γ increases from 0.3 to 0.7, the fraction of the chiral pattern increases.

stronger. This phenomenon is analogous to the geometrical frustration of pentagons, which have fivefold symmetry and are mismatched to 2D crystalline symmetries. If pentagons have a strong orientational correlation between their neighbors by forming side-to-side contacts at high densities, they can neither tile the 2D space periodically nor develop long-range order.

V. CONCLUSION

We have performed wax-snowman packing experiments and BD simulations to investigate the the structure of dense random packing of 2D snowmanlike particles at the individual particle level. The snowman packing experiments revealed that asymmetric snowman particles are strongly correlated in orientation with the surrounding particles and thus prefer to locally form certain types of conformations near the maximally random jammed (MRJ) fraction. There were four types of patterns: parallel, antiparallel I and II, and chiral. We found that the chiral ordering, which does not fit 2D crystalline symmetries, is dominant in the random packing structure. Additionally, BD simulation results showed that the preference for chiral ordering is not affected by the short-range interaction between particles and increases with γ. These findings suggest that the chiral ordering inhibits the development of spatial order of the system due to the mismatch of its geometry with 2D symmetries.

While the snowman shape does not interfere with the 2D crystalline symmetries and can construct several 2D periodic structures, the shape favors unexpected chiral ordering and there is consequently a mismatch between locally preferred structures and 2D crystalline symmetries. Shedding light on why the chiral structure is more dominant rather than the other conformations will be interesting future work, and related findings may provide the possibility to modulate the phases of snowmen by minimizing the chiral ordering and developing spatial order.

ACKNOWLEDGMENTS

This work was supported by the Brain Korea 21 (BK21) project of the Korean government, a grant from the Korea Healthcare Technology R&D Project (Grant No. A040041), the WCU Program through the NRF (Grant No. R33-2008-000-10163-0), the Basic Science Research Program (Grant No. 2009-0087691), the NRF (Grants No. 2011-0031931, No. 2011-0030923, No. 2012R1A1A1011023, and No. 2012R1A6A3A04040395), and the KAIST HRHRP (Grant No. N10110077). M. W. Kim would like to acknowledge support from National Creative Research initiatives of MEST/NRF of Korea (Center for Single-Molecule Systems Biology at KAIST).

[1] K. Zahn, R. Lenke, and G. Maret, Phys. Rev. Lett. **82**, 2721 (1999).
[2] G. Parisi and F. Zamponi, Rev. Mod. Phys. **82**, 789 (2010).
[3] A. Donev, J. Appl. Phys. **95**, 989 (2004).
[4] S. Torquato and F. Stillinger, Rev. Mod. Phys. **82**, 2633 (2010).
[5] H. Tanaka, T. Kawasaki, H. Shintani, and K. Watanabe, Nat. Mater. **9**, 324 (2010).
[6] J. Russo and H. Tanaka, Sci. Rep. **2**, 505 (2012).
[7] K. J. Strandburg, Rev. Mod. Phys. **60**, 161 (1988).
[8] M. E. Cates, J. P. Wittmer, J.-P. Bouchaud, and P. Claudin, Phys. Rev. Lett. **81**, 1841 (1998).
[9] A. Liu and S. Nagel, Nature (London) **396**, 21 (1998).
[10] C. S. O'Hern, L. E. Silbert, A. J. Liu, and S. R. Nagel, Phys. Rev. E **68**, 011306 (2003).
[11] G. Adam and J. H. Gibbs, J. Chem. Phys. **43**, 139 (1965).
[12] M. Ediger, C. Angell, and S. Nagel, J. Phys. Chem. **100**, 13200 (1996).
[13] P. G. Debenedetti and F. H. Stillinger, Nature (London) **410**, 259 (2001).
[14] J. A. Cuesta and D. Frenkel, Phys. Rev. A **42**, 2126 (1990).
[15] I. C. Rankenburg and R. J. Zieve, Phys. Rev. E **63**, 061303 (2001).
[16] T. Schilling, S. Pronk, B. Mulder, and D. Frenkel, Phys. Rev. E **71**, 036138 (2005).
[17] Roel P. A. Dullens, Maurice C. D Mourad, Dirk G. A. L. Aarts, J. P. Hoogenboom, and W. K. Kegel, Phys. Rev. Lett. **96**, 028304 (2006).
[18] L. Filion and M. Dijkstra, Phys. Rev. E **79**, 046714 (2009).
[19] K. Zhao and T. G. Mason, Phys. Rev. Lett. **103**, 208302 (2009).
[20] C. F. Schreck, N. Xu, and C. S. O'Hern, Soft Matter **6**, 2960 (2010).
[21] K. Zhao, R. Bruinsma, and T. Mason, Proc. Natl. Acad. Sci. USA **108**, 2684 (2011).
[22] T. Shen, C. Schreck, B. Chakraborty, D. E. Freed, and C. S. O'Hern, Phys. Rev. E **86**, 041303 (2012).
[23] Y. Han and M. W. Kim, Soft Matter **8**, 9015 (2012).
[24] C. N. Likos and C. L. Henley, Philos. Mag. B **68**, 85 (1993).
[25] T. Kennedy, Discrete Comput. Geom. **35**, 255 (2005).
[26] R. J. Speedy, J. Chem. Phys. **110**, 4559 (1999).
[27] A. Donev, F. H. Stillinger, and S. Torquato, Phys. Rev. Lett. **96**, 225502 (2006).
[28] A. Donev, F. H. Stillinger, and S. Torquato, J. Chem. Phys. **127**, 124509 (2007).
[29] X. Xu and S. A. Rice, Phys. Rev. E **83**, 021120 (2011).
[30] O. Velev, N. Denkov, V. Paunov, P. Kralchevsky, and K. Nagayama, Langmuir **9**, 3702 (1993).
[31] P. A. Kralchevsky and K. Nagayama, Adv. Colloid Interface Sci. **85**, 145 (2000).
[32] D. Vella and L. Mahadevan, Am. J. Phys. **73**, 817 (2005).
[33] Edited by H. C. Ottinger, *Stochastic Processes in Polymeric Fluids* (Springer-Verlag, New York, 1996).
[34] S. H. Lee, S. J. Gerbode, B. S. John, A. K. Wolfgang, F. A. Escobedo, I. Cohen, and C. M. Liddell, J. Mater. Chem. **18**, 4912 (2008).